Article

Cell Reports

Oscillatory Activity in Developing Prefrontal Networks Results from Theta-Gamma-Modulated Synaptic Inputs

Graphical Abstract

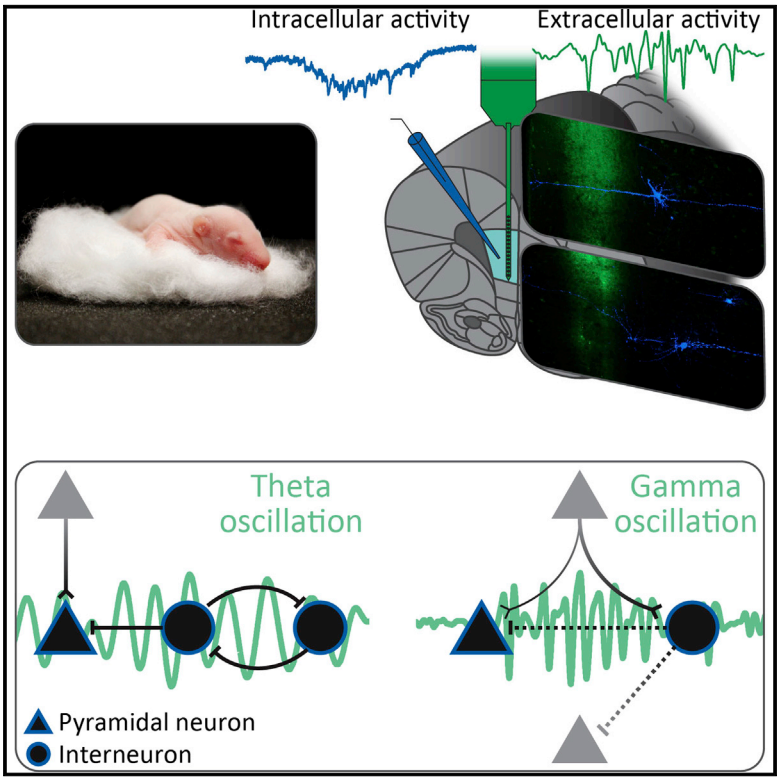

Authors

Sebastian H. Bitzenhofer, Kay Sieben, ..., Marc Spehr, Ileana L. Hanganu-Opatz

Correspondence

hangop@zmnh.uni-hamburg.de

In Brief

Maturation of prefrontal hippocampal communication, a basis for cognitive abilities, depends on co-activation of neuronal networks in oscillatory rhythms. Bitzenhofer et al. identify the cellular substrate of these neonatal oscillations in vivo. While excitation of prefrontal pyramidal neurons is timed by theta activity, beta-low gamma oscillations require glutamatergic drive on interneurons.

Highlights

- Neonatal pyramidal neurons and interneurons have distinct bursting patterns in vivo
- Excitation of prelimbic pyramidal neurons contributes to neonatal theta oscillations
- Neonatal beta-low gamma activity relies on glutamatergic drive on interneurons
- Neonatal high-frequency oscillations are independent of synaptic interactions

Bitzenhofer et al., 2015, Cell Reports *11*, 486–497
April 21, 2015
http://dx.doi.org/10.1016/j.celrep.2015.03.031

CellPress

OPEN ACCESS
CellPress

Cell Reports
Article

Oscillatory Activity in Developing Prefrontal Networks Results from Theta-Gamma-Modulated Synaptic Inputs

Sebastian H. Bitzenhofer,[1,3] Kay Sieben,[1,3] Kai D. Siebert,[1] Marc Spehr,[2] and Ileana L. Hanganu-Opatz[1,*]
[1]Developmental Neurophysiology, Institute of Neuroanatomy, University Medical Center Hamburg-Eppendorf, 20251 Hamburg, Germany
[2]Department of Chemosensation, Institute for Biology II, RWTH Aachen University, 52074 Aachen, Germany
[3]Co-first author
*Correspondence: hangop@zmnh.uni-hamburg.de
http://dx.doi.org/10.1016/j.celrep.2015.03.031

SUMMARY

The hippocampus-driven entrainment of neonatal prefrontal circuits in theta-gamma oscillations contributes to the maturation of cognitive abilities, yet the underlying synaptic mechanisms are still unknown. Here we combine patch-clamp recordings from morphologically and neurochemically characterized layer V pyramidal neurons and interneurons in vivo, with extracellular recordings from the prelimbic cortex (PL) of awake and lightly anesthetized neonatal rats, to elucidate the synaptic framework of early network oscillations. We demonstrate that all neurons spontaneously fire bursts of action potentials. They receive barrages of fast and slow glutamatergic as well as GABAergic synaptic inputs. Oscillatory theta activity results from long-range coupling of pyramidal neurons, presumably within prelimbic-hippocampal circuits, and from local interactions between interneurons. In contrast, beta-low gamma activity requires external glutamatergic drive on prelimbic interneurons. High-frequency oscillations in layer V are independent of interactions at chemical synapses. Thus, specific theta-gamma-modulated synaptic interactions represent the substrate of network oscillations in the developing PL.

INTRODUCTION

Distinct patterns of rhythmic activity organize the neuronal networks during early development (Hanganu-Opatz, 2010; Khazipov and Luhmann, 2006). Increasing experimental evidence indicates that these early network oscillations contribute to the wiring of local and long-range circuits and facilitate the maturation of corresponding behavioral abilities. In sensory cortices, oscillations enable the coupling of neurons within topographic functional units that might act as transient spatio-temporal templates of later-emerging maps (Dupont et al., 2006; Minlebaev et al., 2011; Yang et al., 2013). The development of cognitive processing equally relies on early network oscillations with a complex temporal and spatial organization. The directed theta-band-modulated communication within neonatal prefrontal hippocampal networks seems to control the mnemonic performance at juvenile age (Brockmann et al., 2011; Krüger et al., 2012). Moreover, synchronized network activity in the developing entorhinal cortex (J. Dawitz et al., 2012, Eighth FENS Forum Neurosci., abstract) has been proposed to facilitate the tuning of circuitry necessary for adult grid firing (Hafting et al., 2005; Langston et al., 2010).

Several patterns of oscillatory activity have been described in the developing brain of both humans and animals. While all these patterns share a discontinuous temporal structure that differentiates them from the adult network activity, their properties, especially the frequency range, vary considerably. The ubiquitous spindle bursts with dominant frequencies in the theta-alpha (4–12 Hz) band are accompanied by fast beta-low gamma oscillations (15–50 Hz) as well as by high-frequency oscillations (HFO, 100–400 Hz) (Cichon et al., 2014; Colonnese and Khazipov, 2010; Hanganu et al., 2006; Minlebaev et al., 2011; Yang et al., 2009). Recently, theta-gamma oscillations, defined as nested gamma spindle bursts, have been characterized in the prefrontal cortex (PFC) of neonatal rodents (Brockmann et al., 2011). Despite increasing knowledge of the spatio-temporal structure and function of the diverse neonatal rhythms, their underlying synaptic mechanisms in vivo are largely unknown. The elucidation of these mechanisms bears great potential for dissecting the cortical wiring and information processing during development and for understanding disease-related miswiring. For example, early gamma oscillations in the barrel cortex are mainly driven by excitatory thalamic inputs on neurons in the granular layer and facilitate multiple replays of sensory inputs (Minlebaev et al., 2011). This mechanism is unique during development and differentiates neonatal gamma oscillations from the adult inhibition-based gamma activity (Bartos et al., 2007; Buzsáki, 2002). Taking into account the powerful computational function of theta-gamma oscillations within prefrontal hippocampal networks, which at adulthood account for temporal encoding of information and communication through synchrony (Akam and Kullmann, 2014; Freund and Antal, 1988; Lisman and Jensen, 2013), it is critical to understand their ontogenetic mechanisms.

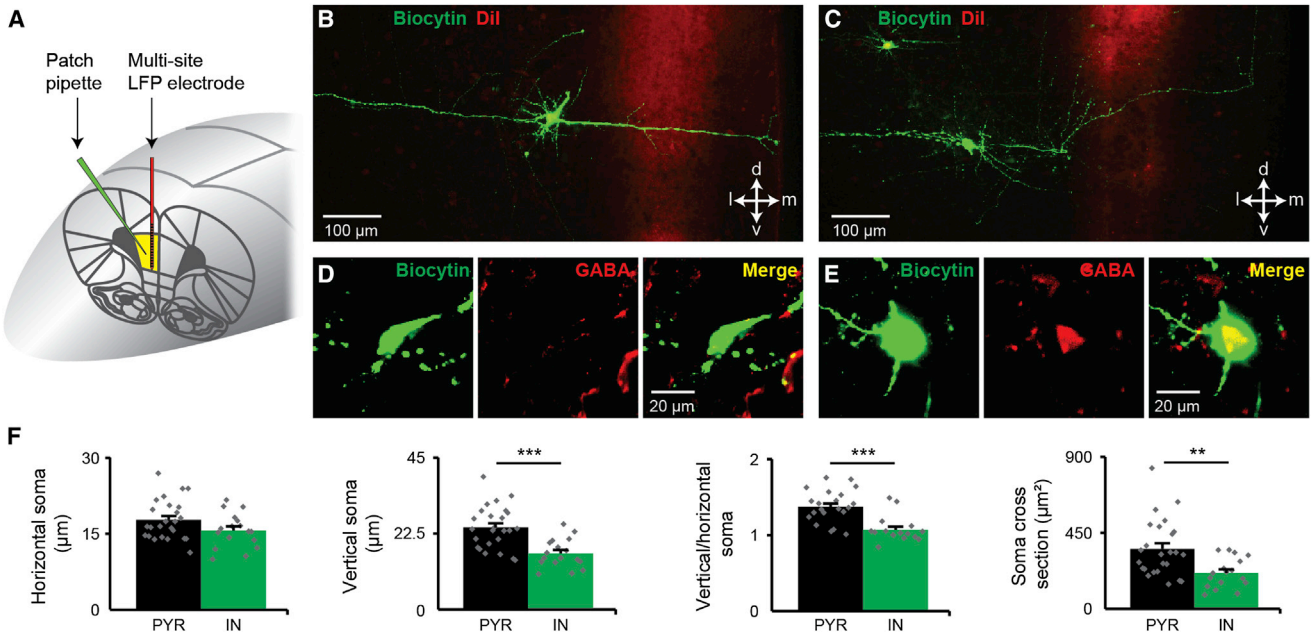

Figure 1. Morphological and Immunohistochemical Characterization of Neurons in the Neonatal PL

(A) Schematic drawing shows the recording configuration allowing positioning the glass pipette for patch-clamp recordings (green) in close proximity to the multi-site LFP electrode (red) in the PL (yellow area).

(B) Morphological classification of biocytin-filled PYRs in the neonatal rat PL. Digital photomontage reconstructs by high-resolution confocal imaging the location of the DiI-labeled multi-site electrode for LFP recordings (red) and the morphology of a biocytin-filled and streptavidin-Cy2-stained PYR (green) in a 400-µm-thick coronal slice including the PL (orientation: d, dorsal; m, medial; v, ventral; and l, lateral). Note the long primary dendrite oriented toward the pial surface and the opposite location of the axon.

(C) Shows the same as (B) for a representative multipolar IN.

(D) GABA immunoreactivity in PYRs via digital images of a biocytin-stained PYR (green, left) after staining for GABA (red, middle). Merged image (right) shows the absence of GABA immunoreactivity in PYR.

(E) GABA immunoreactivity in INs via digital images of a biocytin-stained IN (green, left) after staining for GABA (red, middle). Merged image (yellow, right) reveals high GABA expression that is mainly confined to the soma.

(F) Bar diagrams (mean ± SEM) display the horizontal and vertical sizes of the soma, the ratio of vertical/horizontal soma size, as well as the area of the soma when averaged for all investigated PYRs (black) and INs (green). Gray dots correspond to individual values.

Adult theta oscillations are driven by cholinergic and GABAergic inputs (Freund and Antal, 1988), whereas gamma oscillations mainly emerge within feedforward inhibitory microcircuits including parvalbumin-positive fast-spiking interneurons (INs) (Cardin et al., 2009; Hu et al., 2014; Pernía-Andrade and Jonas, 2014; Sohal et al., 2009; Womelsdorf et al., 2014). To decide whether developing networks have a similar substrate, key questions remain to be answered. First, what are the firing patterns of different neuronal subpopulations in the neonatal PFC in vivo? These patterns have been characterized solely in vitro (Yang et al., 2014), in the absence of major excitatory drives, such as from the hippocampus (HP). Second, how do synaptic inputs on pyramidal neurons (PYRs) and INs contribute to the generation of early network oscillations? Third, how does the firing of distinct neuronal populations in the developing cortex temporally relate to these oscillations? To address these questions, we performed local field potential (LFP) and whole-cell patch-clamp recordings in vivo from biocytin-stained and immunhistochemically characterized neurons in the prelimbic subdivision of the PFC in neonatal rats. Since the theta drive from the hippocampal CA1 area entrains the prelimbic cortex (PL) in oscillatory rhythms via axonal projections that mainly target prelimbic layer V, neurons of this layer were investigated during the developmental stage of maximal drive (i.e., end of the first postnatal week). The present results uncover the cellular interactions contributing to early theta and beta-low gamma oscillations.

RESULTS

The Active Membrane Properties of Prelimbic Neurons Relate to Defined Morphological and Immunohistochemical Profiles

We first characterized the intrinsic properties of prelimbic neurons in vivo at postnatal days (P) 6–8, which represents the developmental stage of maximal drive from the hippocampal CA1 (Brockmann et al., 2011). For this, we performed whole-cell patch-clamp recordings from biocytin-stained neurons in layer V of the PL (n = 42 cells) (Figure 1A). Detailed reconstruction of their morphology combined with immunohistochemistry allowed the classification of recorded neurons into two groups. PYRs had an elongated (horizontal soma diameter: 17.7 ± 0.8 µm, vertical soma diameter: 24.3 ± 1.3 µm) tripolar soma with the major dendrite oriented toward the pial surface and

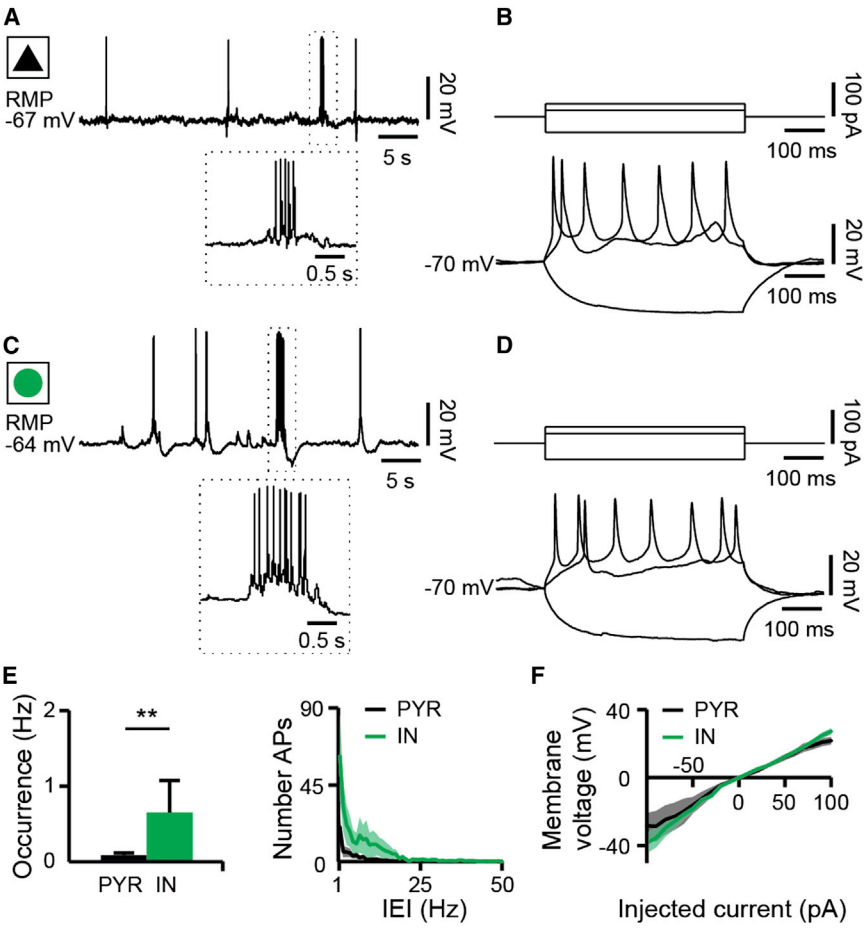

Figure 2. Firing Patterns and Current-Voltage Relationships of PYR (Black Triangle) and IN (Green Circle) in the PL of Neonatal Rats

(A) Representative recording shows the membrane potential from a PYR with single and burst (dotted box, inset) discharges of action potentials.

(B) Voltage responses to the injection of hyper- and depolarizing current pulses at a holding membrane potential of −70 mV. Suprathreshold current pulses elicited repetitive APs.

(C and D) Show the same as (A and B) for an IN.

(E) Bar diagrams (mean ± SEM) display the mean occurrence of spontaneous APs (left) and histograms show the preferred instantaneous frequency (right) for PYRs (black) and INs (green). Note that the IN firing rate peaks at ~6 Hz.

(F) Current-voltage relationships of all investigated PYRs (black) and INs (green). Shaded areas correspond to SEM (See also Figure S1 and Table S1.)

were negative for GABA staining (n = 25) (Figures 1B and 1D). In contrast, GABA-positive neurons that had a multipolar morphology with a round (horizontal soma diameter: 15.7 ± 0.8 μm, vertical soma diameter: 16.6 ± 1 μm) soma of smaller size and multiple primary dendrites with no preferential orientation (n = 17) were classified as INs (Figures 1C, 1E, and 1F). Their axonal projections targeted either the upper layers or were confined to layer V of the PL.

Both neuronal groups showed similar passive membrane properties (Table S1) with resting membrane potentials (RMPs) of −67.3 ± 1.3 mV for PYRs and −64 ± 2 mV for INs, which were similar to previously recorded in vitro values (Yang et al., 2014; Zhang, 2004). At RMP, all investigated neurons generated single and bursts of action potentials (APs) and lacked up-down state transitions, similar to neurons in the neonatal visual cortex (Colonnese, 2014). However, the overall frequency of spontaneous firing was significantly higher ($p = 0.003$) for INs (0.65 ± 0.42 Hz) compared to PYRs (0.09 ± 0.03 Hz). The fraction of burst-organized APs (>25 Hz) versus single spikes was also significantly higher ($p = 0.009$) for INs (0.22 ± 0.16) than PYRs (0.03 ± 0.02), and only INs generated bursts of APs with high discharge frequency (>50 Hz, fraction 0.12 ± 0.11 of the total firing) (Figures 2A, 2C, and 2E; Figure S1; Table S1). In response to sustained depolarization by intracellular current injection, all neurons responded with regular firing at frequencies between 2 and 14 Hz (Figures 2B and 2D). In both groups of neurons, the voltage deflection showed linear dependence on the injected current (Figure 2F). All INs lacked a hyperpolarization-activated voltage sag, suggesting the absence of an h-current (I_h). Only one recorded PYR showed such a low-amplitude sag. Thus, morphologically and immunohistochemically characterized PYRs and INs have similar passive membrane and AP properties, but distinct bursting patterns in the neonatal PL in vivo.

PYRs and INs in the Neonatal PL Receive Strong Barrages of Synaptic Inputs

In a first attempt to elucidate the cellular interactions within the neonatal PL, we investigated the excitatory postsynaptic currents (EPSCs) under voltage-clamp conditions at a holding potential of −70 mV, which corresponds to the reversal potential of $GABA_A$ receptor-mediated currents. All neurons received glutamatergic EPSCs, which were mainly organized as high-frequency burst-like discharges (Figures 3A and 3B). Unsupervised detection and analysis confirmed by visual inspection revealed that the EPSCs occurred significantly more frequently ($p = 0.014$) in INs (2.16 ± 0.45 Hz) than in PYRs (0.98 ± 0.24 Hz), although the amplitudes were similar for both groups (PYR: 13.63 ± 0.44 pA, IN: 14.4 ± 1.07 pA; $p = 0.56$) (Figure S2). Furthermore, the EPSCs in PYRs and INs had different kinetics. While PYRs predominantly received EPSCs with fast decay that could be best fitted by a monoexponential function (decay time constant [τ] 8.85 ± 1.45 ms), monoexponential fast (τ: 6.1 ± 0.42 ms) and biexponential slow (τ_1: 8.14 ± 1.01 ms, relative amplitude −9.98 ± 1.51; τ_2: 54.4 ± 11.1 ms, relative amplitude −5.09 ± 0.6) EPSCs could be recorded in INs (Figures 3A–3E;

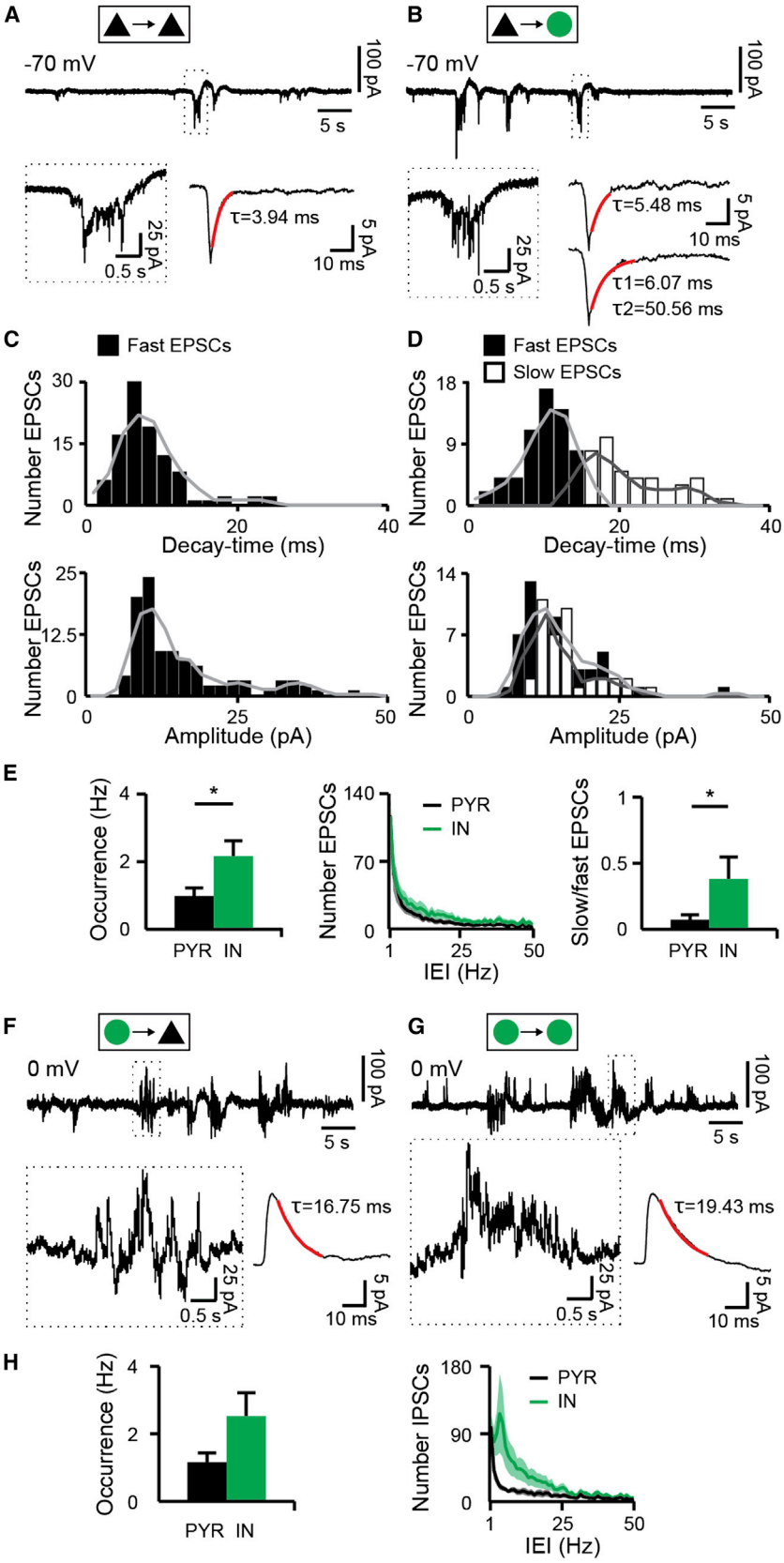

Figure 3. Synaptic Inputs on PYRs and INs in the Neonatal PL

(A) (Top) Representative trace recorded at −70 mV from a PYR (black triangle). Note the strong barrage of glutamatergic EPSCs (dotted box, inset). (Bottom) Averaged EPSCs (n = 100 events) are fitted with a monoexponential function (red line). Note the fast kinetics of EPSCs in PYRs.

(B) (Top) Representative trace recorded at −70 mV from an IN (green circle). (Inset) Barrage of glutamatergic EPSCs is displayed at a larger scale (dotted box). (Bottom) Averaged fast (n = 62 events, top) and slow (n = 38 events, bottom) EPSCs are fitted with a monoexponential and a biexponential function (red lines), respectively.

(C) Histograms show the decay-time (top) and amplitude (bottom) distributions obtained from the EPSCs (n = 100 events) recorded from a P7 PYR. Note the unimodal decay and amplitude distributions.

(D) Shows the same as (C) for EPSCs (n = 100 events) recorded from a P7 IN. Note the bimodal decay distribution corresponding to fast and slow EPSCs. For (C) and (D), the gray lines superimposed on the histograms represent the moving average.

(E) (Left) Bar diagram (mean ± SEM) displays the averaged occurrence of EPSCs in PYRs and INs. (Middle) Histogram shows the instantaneous frequency distribution of EPSCs in PYRs and INs. (Right) Bar diagram (mean ± SEM) displays the ratio of slow versus fast EPSCs in PYRs and INs.

(F) (Top) Representative trace recorded at 0 mV from a PYR (black triangle). Note the strong barrage of GABAergic IPSCs (dotted box, inset). (Bottom) Averaged IPSCs (n = 100 events) are fitted with a monoexponential function (red line).

(G) (Top) Representative trace recorded at 0 mV from an IN (green circle). (Inset) Barrage of GABAergic IPSCs is displayed at a larger scale (dotted box). (Bottom) Averaged IPSCs (n = 100 events, bottom) are fitted with a monoexponential function (red line).

(H) (Left) Bar diagram (mean ± SEM) displays the averaged occurrence of IPSCs in PYRs and INs. (Right) Histogram shows the instantaneous frequency distribution of IPSCs in PYRs and INs. (See also Figure S2.)

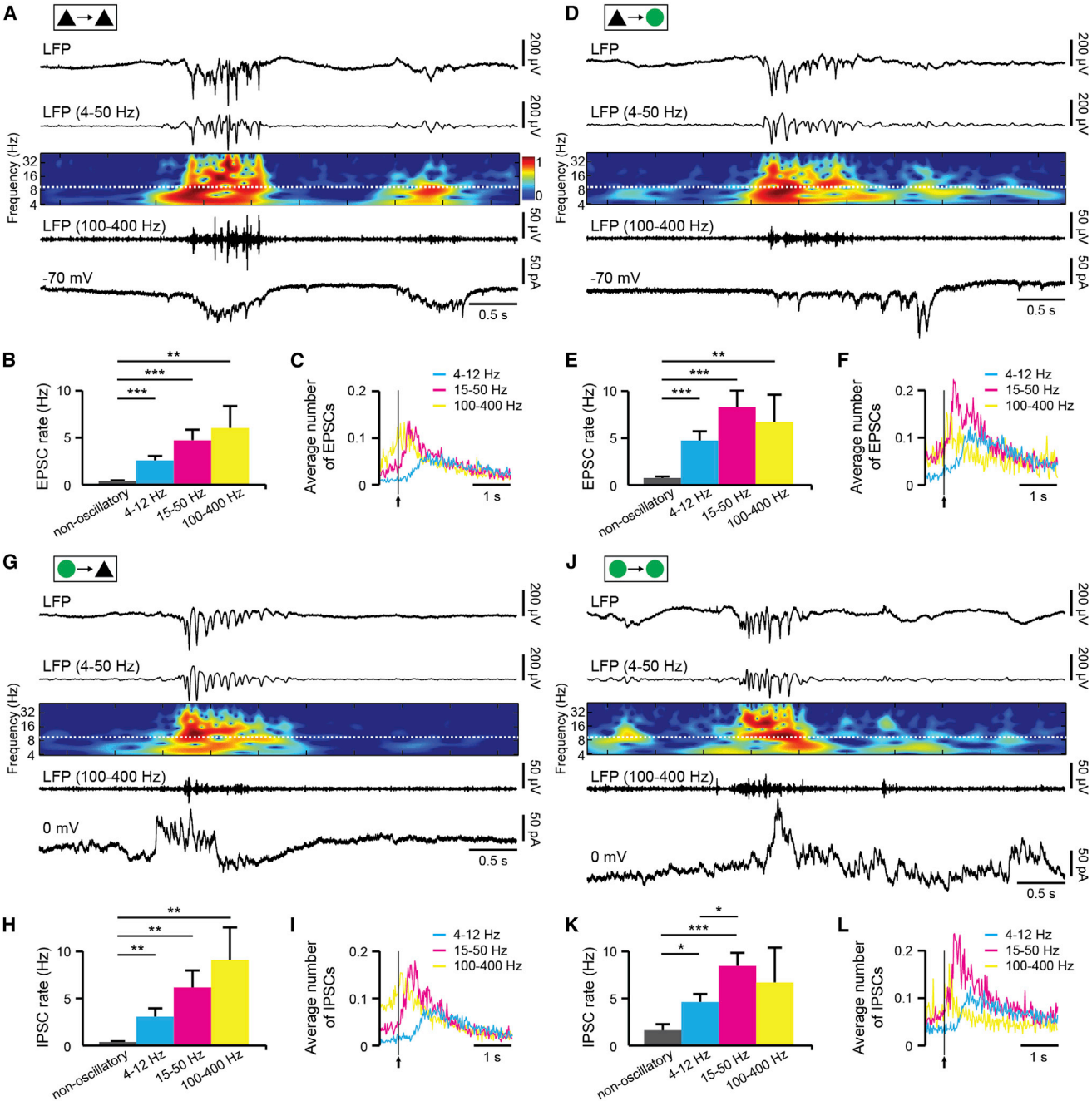

Figure 4. Temporal Relationships between Network Oscillations and Synaptic Activity in the Neonatal PL

(A) Simultaneous recordings of the LFP and EPSCs on a PYR in the PL of a P8 rat. Characteristic nested-gamma spindle burst (NG) displayed before (top) and after band-pass (4–50 and 100–400 Hz) filtering (middle) together with the color-coded frequency plot of the LFP wavelet spectrum. (Bottom) Glutamatergic EPSCs were recorded simultaneously with the LFP at −70 mV in whole-cell voltage-clamp configuration. Note the temporal correlation between the NG and EPSCs.

(B) Bar diagram (mean ± SEM) shows the EPSCs occurrence during network oscillations (theta, beta-low gamma, and HFOs) compared with non-oscillatory time windows.

(C) Histograms show LFP-triggered synaptic currents for theta (cyan), beta-low gamma (magenta), and HFO (yellow) oscillatory components. The black arrow and line mark the oscillation onset.

(D–F) Show the same as (A–C) for EPSCs on an IN in the PL of a P7 rat.

(G) Simultaneous recordings of the LFP and IPSCs on a PYR in the PL of a P6 rat. Characteristic NG is displayed before (top) and after band-pass (4–50 and 100–400 Hz) filtering (middle) together with the color-coded frequency plot of the LFP wavelet spectrum. (Bottom) IPSCs were recorded simultaneously with the LFP at 0 mV in whole-cell voltage-clamp configuration. Note the temporal correlation between the NG and IPSCs.

(legend continued on next page)

Figure S2A). The ratio of fast to slow EPSCs in INs was 4:1. Both fast and slow EPSCs showed a unimodal amplitude distribution. The absence of significant correlations between the distribution of EPSCs rise time and amplitude and between EPSCs rise and decay times suggests that dendritic cable filtering did not substantially influence the kinetics of neonatal synaptic events (Figures S2B and S2C).

In a second step, whole-cell voltage-clamp recordings at 0 mV, which corresponds to the reversal potential of glutamate receptor-mediated currents, enabled the investigation of inhibitory postsynaptic currents (IPSCs) in both PYRs and INs of the neonatal PL. The depolarizing, but shunting inhibitory action of GABA at neonatal age (K. Kirmse et al., 2014, Soc. Neurosci., conference) justifies this nomenclature for GABAergic inputs. Similar to EPSCs, the GABAergic IPSCs in PYRs and INs were organized in barrages of synaptic events (Figures 3F and 3G). Their occurrence (PYR: 1.15 ± 0.28 Hz, IN: 2.51 ± 0.7 Hz; $p = 0.093$), amplitude (PYR: 23 ± 3.7 pA, IN: 22.5 ± 3.5 pA; $p = 0.62$), and decay time (PYR: 14 ± 1.31 ms, IN: 17.7 ± 2 ms; $p = 0.17$) were similar for both neuronal groups (Figure 3H; Figure S2A). The inter-event interval (IEI) of IPSCs in INs, but not in PYRs, showed a pronounced instantaneous frequency-dependent distribution with a peak at ~6 Hz. Similar theta-band-confined distribution of IEI was observed for interneuronal APs (Figure 2E), suggesting that local IN-IN circuits within prelimbic layer V may contribute to theta oscillations.

Taken together, our results indicate that, at the end of the first postnatal week, both prelimbic PYRs and INs receive bursts of excitatory and inhibitory synaptic currents.

Timing of Synaptic Inputs by Network Oscillations Is Cell and Frequency Specific in the Neonatal PL

To decide whether synaptic inputs on PYRs and INs contribute to the generation of different oscillatory patterns in the neonatal PL, we simultaneously recorded the LFP in close proximity to patched neurons in vivo. As previously reported (Bitzenhofer and Hanganu-Opatz, 2014; Brockmann et al., 2011), the network activity of the neonatal PL was discontinuous, i.e., oscillations switching between different frequency components alternated with long periods of network silence (Figure 4; Figure S3A). Unsupervised detection and categorization using the features of discontinuous oscillations confirmed the presence of two activity patterns: (1) spindle bursts with a single theta-confined frequency component, and (2) nested gamma spindle bursts with distinct theta- (4–12 Hz) and beta-low gamma-confined (15–50 Hz) frequency components, which were superimposed with low-amplitude nested HFOs (100–400 Hz) (Cichon et al., 2014). Cross-frequency coherence revealed the tight coupling between the phase of theta component and the amplitude of beta-low gamma component as well as between the phase of beta-low gamma component and the amplitude of HFOs (Figure S4). In line with previous findings from primary sensory cortices (Yang et al., 2009), the patterns of oscillatory activity were similar in awake ($n = 5$) and urethane-anesthetized P6–8 rats ($n = 5$), with only slightly reduced amplitudes ($p = 0.049$) under anesthesia (Figure S5). The similarity might be due to the ability of urethane to mimic sleep conditions (Clement et al., 2008), the dominant behavioral state of neonatal rats. Consequently, subsequent investigations were performed under light urethane anesthesia.

Despite the fragility of the neonatal skull and brain, the prelimbic patterns of oscillatory activity were not affected in their occurrence, amplitude, duration, and spectral distribution by the insertion of the patch pipette into the PL at 50–400 μm from the multi-site extracellular electrode (Figure S3C). The long-lasting stability of paired patch-clamp and LFP recordings from neonatal rats enabled precise examination of the timing of synaptic currents by network oscillations in vivo (Figures 4 and 5). In a first step, we analyzed the occurrence of synaptic events during oscillations. The highest rates of discharge for glutamatergic and GABAergic inputs were confined to the time windows of network oscillations (PYR EPSCs: 3.3 ± 0.7 Hz, PYR IPSCs: 4.2 ± 1.1 Hz; IN EPSCs: 6.1 ± 1.3 Hz, IN IPSCs: 6.1 ± 1.1 Hz), whereas their occurrence was comparable and extremely low during periods of network silence (PYR EPSCs: 0.4 ± 0.1 Hz, PYR IPSCs: 0.4 ± 0.1 Hz; IN EPSCs: 0.9 ± 0.2 Hz, IN IPSCs: 1.8 ± 0.6 Hz). The occurrence of synaptic inputs in relationship to the spectral structure of network oscillations was high during all frequency components of LFP oscillations (Figures 4B, 4E, 4H, and 4K). When calculating the histograms of LFP-triggered synaptic inputs (Figure S6A), we observed that the rise in the occurrence of synaptic activity in both PYRs and INs occurred shortly after the onset of theta (PYR EPSCs: 80 ms, PYR IPSCs: 40 ms; IN EPSCs: 40 ms, IN IPSCs: 180 ms) and beta-low gamma activity (PYR EPSCS: 120 ms, PYR IPSCs: 80 ms; IN EPSCs: 40 ms, IN IPSCs: 60 ms) (Figures 4C, 4F, 4I, and 4L). Similar augmentation was detected during HFOs.

In a second step, we assessed the timing of synaptic inputs by the ongoing network oscillations in the neonatal PL. For this, we computed for each oscillatory component (theta, beta-low gamma, and HFOs) the average of the LFP triggered at the peak time of intracellular synaptic currents (Figure S6B). If synaptic inputs contribute to the LFP in a specific frequency band, they will not be randomly distributed, but will preferentially concentrate at a defined phase of the oscillatory cycle. The synaptic inputs in PYRs were phase locked to the theta band component of oscillatory activity. While the EPSCs occurred mainly at the descending phase of the oscillatory cycle, the IPSCs occurred mainly at its trough with a delay of ~18 ms (Figures 5A and 5D). In PYRs, the EPSCs were additionally locked to beta-low gamma activity, yet to a lesser extent. These modulatory effects were confirmed by the maximal values of the synaptic-input-triggered LFP average power and oscillation-trough-triggered EPSC or IPSC histograms and were absent

(H) Bar diagram (mean ± SEM) shows the IPSCs occurrence during network oscillations (theta, beta-low gamma, and HFOs) compared with non-oscillatory time windows.

(I) Histograms show oscillation-triggered synaptic currents for theta (cyan), beta-low gamma (magenta), and HFO (yellow) oscillatory components. The black arrow and line mark the oscillation onset.

(J–L) Show the same as (G–I) for IPSCs on an IN in the PL of a P7 rat. (See also Figures S3–S5 and S6A.)

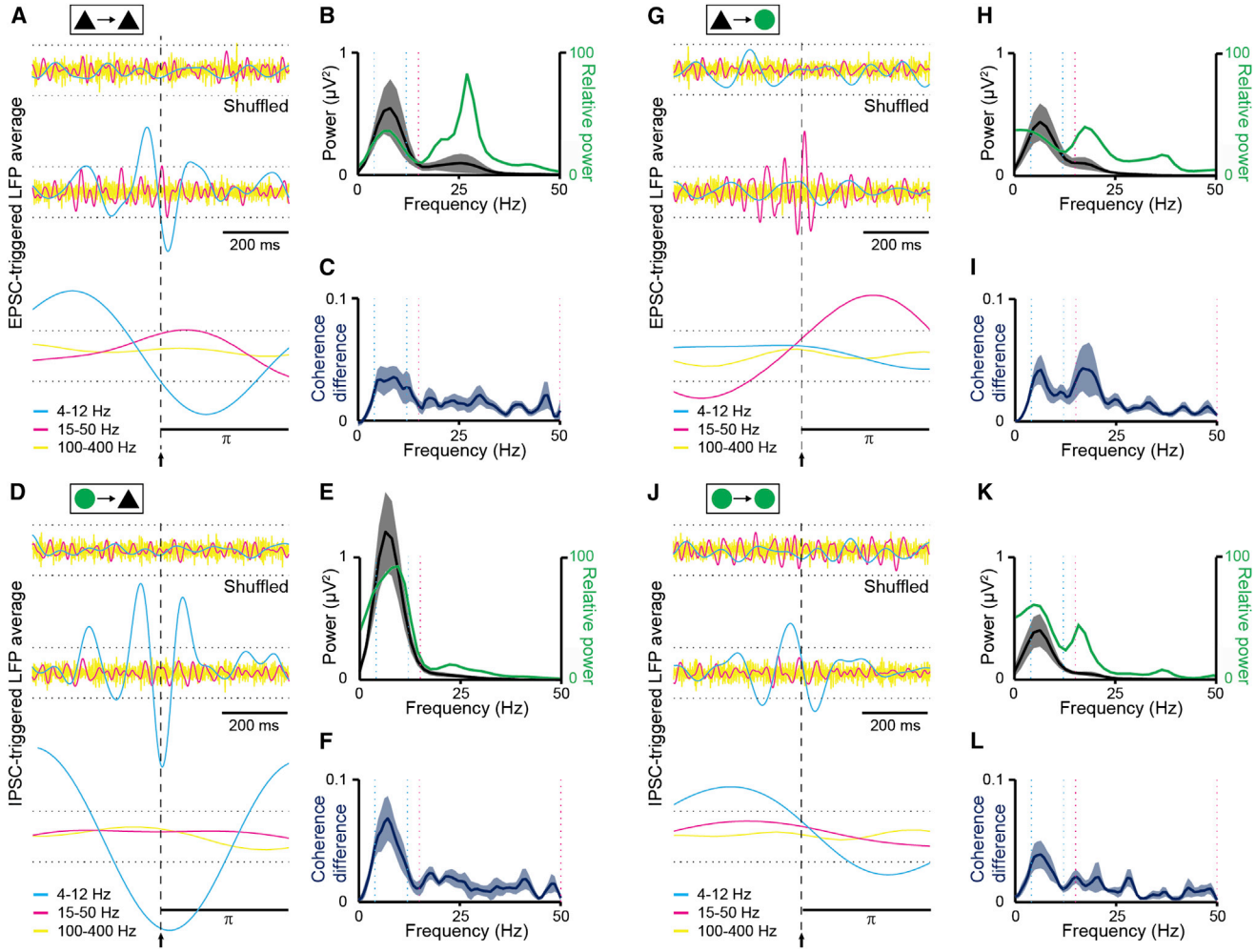

Figure 5. Phase Locking and Coherence Analysis for Synaptic Inputs in Relationship to Network Oscillations in the PL of Neonatal Rats

(A) LFP in different frequency bands is aligned and averaged to the peaks (vertical dashed line) of shuffled (top) and original (middle) EPSCs recorded from PYRs (n = 13). (Bottom) The EPSC-triggered LFP average is displayed for one oscillatory cycle of each frequency band. Note the significant theta modulation of EPSCs. The values are normalized to 99% confidence interval (horizontal dotted lines).

(B) Power spectrum of the EPSC-triggered LFP average is calculated for original data and normalized to the power of shuffled data (green).

(C) Synchrony between EPSC envelope and EPSC-triggered LFP is displayed as coherence difference between original and shuffled data.

(D–F) Show the same as (A–C) for LFP and IPSCs in PYRs.

(G–I) Show the same as (A–C) for LFP and EPSCs in INs (n = 14).

(J–L) Show the same as (A–C) for LFP and IPSCs in INs. For all histograms, the shaded areas correspond to SEM (See also Figures S6B and S7.)

for shuffled data (Figures 5B and 5E; Figure S7). In contrast, the EPSCs in INs were strongly locked to beta-low gamma frequency components and concentrated on the ascending phase of the oscillatory cycle (Figure 5G). Moreover, GABAergic inputs in INs were theta modulated (Figure 5J). None of the analytical approaches detected a temporal relationship between synaptic currents and HFOs in the neonatal PL.

The ability of synaptic inputs to operate at a specific frequency was tested by calculating the relative frequency-resolved coherence between the envelope of barrage-organized synaptic currents and LFP oscillations. The coherence for EPSCs in PYRs, IPSCs in PYRs, and IPSCs in INs peaked within the theta band (8.7, 7.2, and 6.4 Hz), whereas the main coherence peak was detected at 16.7 Hz for EPSCs in INs (Figures 5C, 5F, 5I, and 5L). Thus, despite global augmentation of synaptic activity in all prelimbic neurons during neonatal theta-gamma oscillations and HFOs, the precise temporal coupling between intracellular currents and LFP was cell and frequency specific. GABAergic inputs on PYRs and INs as well as glutamatergic inputs on PYRs correlated with the activity in the theta band, whereas glutamatergic inputs on INs and to a lesser extent on PYRs contributed to oscillations in the beta-low gamma band. The neonatal HFOs were not locked to the synaptic activity of layer V neurons. This independence of chemical synaptic interactions led to the hypothesis that HFOs may result from gap-junctional, possibly axo-axonal, coupling. Our preliminary findings suggest that these electrical

synapses are located outside the investigated layer V, since assessment of dye coupling of PYRs through the contact of processes confined to this layer failed to identify axo-axonal gap junctions.

The Modulation of Neuronal Firing by Network Oscillations Is Cell and Frequency Specific in the Neonatal PL

The contribution of EPSCs and IPSCs on prelimbic PYRs and INs to different frequency components of neonatal oscillations suggests that distinct circuits operate in specific frequency bands already during neonatal development. To dissect the interactions within these circuits, we assessed the temporal organization of pyramidal and interneuronal firing in relationship to theta and beta-low gamma components of the LFP and to HFOs. Similar to the augmented occurrence of synaptic inputs during network activity, spontaneous firing of prelimbic neurons was mainly confined to the time windows of discontinuous oscillations (Figures 6A–6F). However, the temporal relationship between pyramidal/interneuronal firing and oscillatory LFP components was less precise when compared with the LFP-induced modulation of synaptic activity (Figures 6B and 6E). The LFP-triggered AP histograms revealed only a weak correlation between the firing of PYRs/INs and beta-low gamma frequency component (Figures 6C and 6F). In line with the absence of a preferred firing frequency (see Figure 2E), the APs of PYRs were neither phase locked nor coherent with theta or beta-low gamma oscillations (Figures 6G–6I). Since the firing of layer V PYRs was not timed in a frequency-specific manner, these neurons do not seem to account for the generation of theta-modulated EPSCs. In contrast, the AP-triggered LFP average and coherence analysis demonstrated that the interneuronal firing and theta oscillations were temporally correlated (Figures 6J–6L). Even if to a lesser extent, interneuronal APs seem to contribute to beta-low gamma oscillations. No temporal relationship between HFOs and APs of layer V prelimbic neurons was detected. Thus, the firing of prelimbic INs might contribute to the activation of local circuits underlying theta-gamma activity. In contrast, PYRs involved in the generation of oscillatory activity in the PL seem to be located outside the prelimbic layer V.

DISCUSSION

In the adult brain, information processing occurs by dynamic and selective entrainment of neuronal circuits within oscillatory rhythms. Recently, the cellular structure and the frequency-specific processing of these circuits have been characterized in detail (Womelsdorf et al., 2014), yet their ontogeny is less well understood. Via the present study, we elucidated the mechanisms underlying theta-gamma oscillations in the PL of neonatal rats. At this developmental stage, the PL is strongly driven by hippocampal theta bursts via direct glutamatergic axonal projections (Bitzenhofer and Hanganu-Opatz, 2014; Brockmann et al., 2011). Here we show that (1) synaptic mechanisms underlie the generation of discontinuous theta and beta-low gamma oscillatory activity, but not of HFOs, in the neonatal PL; (2) glutamatergic and GABAergic synaptic inputs on layer V PYRs are coherent and phase locked with theta-band activity; (3) glutamatergic synaptic inputs on layer V prelimbic INs are coherent and phase locked with beta-low gamma activity; and (4) the firing of prelimbic INs, but not PYRs, is theta modulated. Taken together, the present results reveal that different spectral components of discontinuous oscillations in the neonatal PL emerge within distinct neuronal circuits and according to development-specific processing rules (Figure 7).

Profile of Prelimbic Neurons during Neonatal Development In Vivo

While the morphological, immunohistochemical, and physiological profiles of prelimbic neurons have been extensively investigated in the adult brain (Lee et al., 2014; Wang et al., 2006), their properties at early stages of development are poorly elucidated and most knowledge originates from in vitro studies (Zhang, 2004). The present investigation of active and passive membrane properties of prelimbic neurons in vivo in relation to the characterization of their morphology and GABA expression aims to fill this knowledge gap. We demonstrate that, despite profound morphological and neurochemical differences between PYRs and INs as well as between INs (e.g., different orientation of axonal projections), the properties of APs from PYRs and INs during neonatal development are similar. All prelimbic neurons fire spontaneously by the end of the first postnatal week, this ability being more pronounced under in vivo than in vitro conditions. Moreover, none of the AP properties (regular spiking pattern upon depolarization, AP amplitude and width) reliably differentiates neonatal PYRs from INs. These findings suggest that, in the neonatal cortex, neither spike shape nor width provides criteria to assign the extracellularly recorded spikes to either PYRs or INs, as commonly done for adult spikes (Csicsvari et al., 1999). In contrast, already at neonatal age, INs, but not PYRs, generate high-frequency burst discharge, similar to adult INs.

Mechanisms Underlying Theta Activity in the Neonatal PL

The theta-band-confined high synchrony and precise phase locking of glutamatergic synaptic inputs on PYRs and the absence of theta modulation of PYR firing suggest that an external excitatory drive on layer V PYRs contributes to the generation of the dominant 4–12 Hz component of discontinuous oscillations in the neonatal PL (Figure 7A). In line with our previous results (Bitzenhofer and Hanganu-Opatz, 2014; Brockmann et al., 2011), this external drive may originate from the HP. The abundant projections from CA1 PYRs to the prelimbic layer V at the end of the first postnatal week have been identified as anatomical substrate of theta-modulated directed communication within prefrontal hippocampal networks (Brockmann et al., 2011). Similar to adult hippocampal activity (Buzsáki, 2002; Pernía-Andrade and Jonas, 2014), discontinuous theta bursts in the neonatal HP rely on a septal pacemaker and an entorhinal relay (Brockmann et al., 2011). The firing of hippocampal PYRs leads to massive discharge of fast, most likely AMPA receptor-mediated EPSCs in prelimbic PYRs. Their coherence with the theta rhythm might indicate that they provide a major contribution to this rhythm within prelimbic hippocampal networks. Besides the HP, the neurons in layer II/III of the neonatal PL may represent

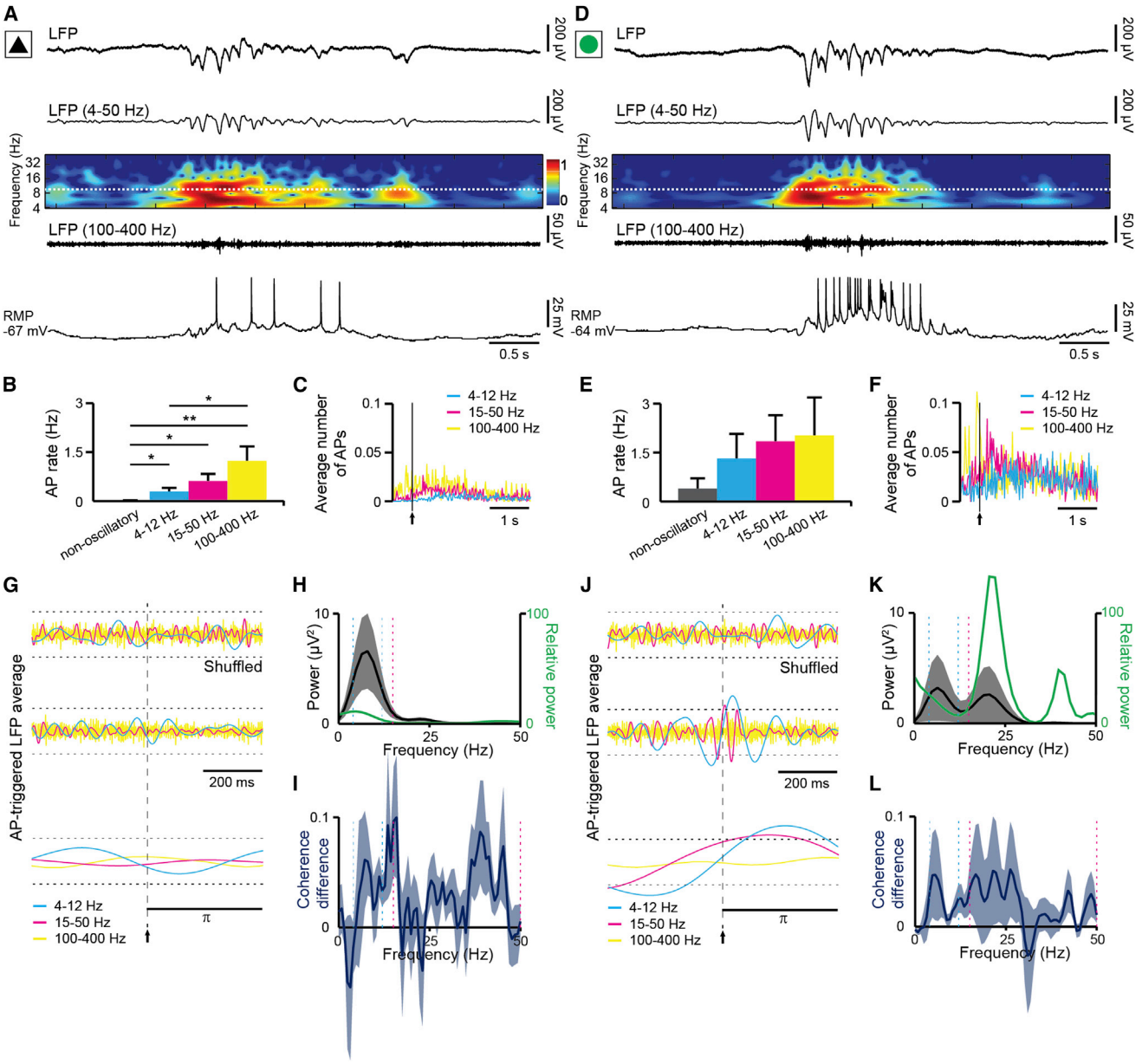

Figure 6. Temporal Relationships between Network Oscillations and APs in the Neonatal PL

(A) Simultaneous recordings of the LFP and APs from a PYR in the PL of a P7 rat. Characteristic NG displayed before (top) and after band-pass (4–50 Hz and 100–400 Hz) filtering (middle) together with the color-coded frequency plot of the LFP wavelet spectrum. (Bottom) Sub-threshold postsynaptic potentials and APs were recorded simultaneously with the LFP at the RMP in whole-cell current-clamp configuration. Note the temporal correlation between NG and AP discharge.

(B) Bar diagram (mean ± SEM) shows the APs occurrence during network oscillations (theta, beta-low gamma, and HFOs) compared with non-oscillatory time windows.

(C) Histograms show LFP-triggered APs for theta (cyan), beta-low gamma (magenta), and HFO (yellow) oscillatory components. The black arrow and line mark the oscillation onset.

(D–F) Show the same as (A–C) for the LFP and APs from INs in the PL of a P7 rat.

(G) LFP in different frequency bands is aligned and averaged to the peaks (vertical dashed lines) of shuffled (top) and original (middle) APs recorded from PYRs (n = 14). (Bottom) The AP-triggered LFP average is displayed for the duration of one oscillatory cycle of each frequency band. The values are normalized to 99% confidence interval (horizontal dotted lines).

(H) Power spectrum of the AP-triggered LFP average is calculated for original data and normalized to the power of shuffled data (green).

(I) Synchrony between AP envelope and AP-triggered LFP is displayed as coherence difference between original and shuffled data.

(J–L) Show the same as (G–I) for the LFP and APs recorded from INs (n = 6). For all histograms, the shaded areas correspond to SEM.

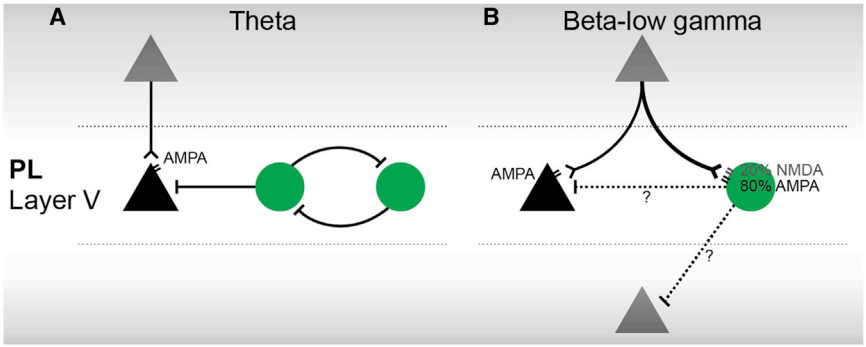

Figure 7. The Circuits Underlying the Frequency Components of Oscillatory Activity in the PL of Neonatal Rats

(A and B) Schematic diagram shows the circuits underlying the theta (A) and beta-low gamma (B) frequency components of oscillatory activity in the PL of neonatal rats. Black and gray triangles correspond to PYRs located inside and outside layer V, respectively, whereas INs are displayed as green circles.

an additional external glutamatergic drive on layer V PYRs. These projections have been reported to become functional around P6 (Zhang, 2004).

The high coherence of IPSCs in INs and interneuronal firing with the theta rhythm indicates that local interneuronal networks confined to layer V may additionally contribute and strengthen the theta activity in the PL. Similar circuits have been described previously in the adult neocortex (Blatow et al., 2003). Their dissection in vitro revealed that the ability of a morphologically and physiologically distinct sub-population of INs to generate theta oscillations critically depends on a strong cholinergic input. Indeed, the cholinergic projections from the basal forebrain selectively target INs, but not PYRs, in the neonatal PL, supporting a selective modulation of interneuronal circuits (Janiesch et al., 2011).

A third mechanism underlying the generation of theta oscillations seems to involve the local layer V-confined coupling of PYRs and INs. The theta-modulated firing of INs results in bursts of GABAergic IPSCs on PYRs that are precisely locked and coherent with the activity in this frequency band. However, in the absence of I_h currents and consequently of spiking resonance in PYRs at neonatal age, it remains unclear which mechanisms amplify the rather weak oscillatory entrainment within this local circuit (Stark et al., 2013).

Mechanisms Underlying Fast Network Activity in the Neonatal PL

The present data indicate that beta-low gamma components of the discontinuous oscillations in the neonatal PL critically require the precise timing of excitation in INs (Figure 7B). The barrages of EPSCs in INs were strongly phase locked at this frequency, inducing beta-low gamma modulation of interneuronal firing. The local impact of this timed firing is less clear, since the GABAergic inputs on PYRs and INs in layer V are not beta-low gamma coherent. The incomplete maturation of both interneuronal projections and neurochemical identity at the end of the first postnatal week (Chu and Anderson, 2015) as well as the diverse origin of GABAergic inputs on PYRs and INs (Karube et al., 2004) and the complexity of PYR-IN interactions (Lee et al., 2014) may account for the lack of beta-low gamma timing. The neonatal interactions between PYRs and INs are highly reminiscent of those defining the emergence of adult gamma activity within an excitation (E)- inhibition (I) model (Bartos et al., 2007; Buzsáki and Wang, 2012; Wang, 2010). Thus, the activating drive from the HP seems to facilitate the local entrainment of prelimbic circuitry (upper layers-layer V) in beta-low gamma oscillations.

The superimposed HFOs represent the unique pattern of neonatal network activity that is generated independently of precisely timed synaptic interactions. Since neither the synaptic activity nor the APs of PYRs and INs are temporally related to HFOs, the question arises of which mechanisms account for their generation. The cross-frequency coherence analysis (Figure S4) confirmed our previous investigation of coupling between phase and spectral signatures (Scheffer-Teixeira et al., 2013), showing that the HFOs represent a distinct form of network activity and not spike-leaked activity (Cichon et al., 2014). On one hand, they might mirror the local entrainment of a local circuit that does not include the patched neurons. On the other hand, the HFOs might be mediated by axo-axonal gap-junctional coupling between PYRs, as previously shown for HFOs in the adult HP (Nimmrich et al., 2005; Schmitz et al., 2001). The augmented occurrence of synaptic inputs during HFOs in the absence of their phase locking may reflect synchronized secondary events or discharges by which the gap-junctional coupling can generate HFOs. Since no dye coupling of PYRs has been detected in layer V, it is likely that the axo-axonal gap junctions are rather sparse and more distally located. Further studies are warranted to shed more light on the mechanisms of HFO generation in the neonatal PL.

Integrative View on Prelimbic Wiring during Development

The present results demonstrate that complex cellular mechanisms are the substrate of network oscillations at neonatal age. Long-range excitation most likely contributes to the prominent theta activity, whereas feedforward inhibition, involving morphologically and neurochemically immature GABAergic neurons within local prelimbic circuitry, seems to account for fast beta-low gamma oscillations (Figure 7). The latency between the phase locking of EPSCs versus IPSCs on the theta cycle supports a feedforward interaction model. GABA has been recently identified as a dual depolarizing-inhibitory neurotransmitter in the immature neocortex in vivo (K. Kirmse et al., 2014, Soc. Neurosci., conference). The induced shunting inhibition in these neurons with a high intracellular chloride concentration (Blaesse et al., 2009; Kilb, 2012) may facilitate the ability of INs to organize the local circuitry responsible for fast activity by homogenizing the firing frequency of PYRs (Vida et al., 2006; Krupa et al., 2014).

The synaptic interactions accounting for theta or beta-low gamma oscillations were mediated by different receptors. The presence of EPSCs with both fast and slow kinetics indicate that AMPA and NMDA receptors mediated the glutamatergic inputs on INs, whereas the external, most likely hippocampal, excitation on layer V PYRs solely relies on AMPA receptors.

By elucidating the cellular substrate of early network oscillations, the present findings reveal the complexity of long-range and local interactions generating the broad spectral structure of neonatal cortical activity. They open the perspective of developmental manipulation of these cellular elements in relationship to later behavioral performance. Understanding the early wiring mechanisms represents a crucial prerequisite for the clarification of miswiring patterns in neurodevelopmental disorders.

EXPERIMENTAL PROCEDURES

All experiments were performed in compliance with the German laws and the guidelines of the European Community for the use of animals in research and were approved by the local ethical committee (111/12, 132/12).

Surgical Preparation and Recordings

Extracellular recordings of the LFP were performed in the PL of P6–8 rats in vivo using previously described experimental protocols (Bitzenhofer and Hanganu-Opatz, 2014; Brockmann et al., 2011; Cichon et al., 2014). Whole-cell patch-clamp recordings were performed using glass pipettes (tip resistance, 3–6 MΩ) that were filled with 125 mM Cs-gluconate, 4 mM CsOH, 1 mM EGTA, 10 mM HEPES, 2 mM $MgCl_2$, and 0.1 mM $CaCl_2$ for voltage-clamp recordings; and 135 mM K-gluconate, 4 mM KCl, 10 mM Na_2-phosphocreatine, 10 mM HEPES, 4 mM MgATP, and 0.3 mM NaGTP for current-clamp recordings. Both solutions were adjusted to pH 7.3 with 1 M CsOH or KOH and to an osmolarity of 306 mOsm with sucrose. In all experiments, 0.5% biocytin (Sigma-Aldrich) was included in the pipette solution for morphological identification of the recorded cells post-mortem. Patch pipettes were obliquely (35° to midline) advanced into the brain to target layer V of the PL (2 mm anterior to bregma, 0.3 mm from midline, 2.7 mm depth). To avoid clotting of the pipette, positive pressure (250 mbar) was applied to the pipette during insertion through the access hole located above the primary motor cortex. Synaptic currents and APs were recorded for at least 240 s using a discontinuous voltage-clamp/current-clamp amplifier (ELC-03XS, npi elektronik).

Dye-coupling (with Rhodamine 123) experiments were performed on a confocal microscope (DM 6000CFS, Leica) using whole-brain coronal slices (300 μm thick) including the PFC of P6–8 rats that were superfused with an extracellular solution containing 145 mM NaCl, 5 mM KCl, 1 mM $CaCl_2$, 1 mM $MgCl_2$, and 10 mM HEPES. Cell-attached recordings were first obtained and the dye coupling was monitored by the acquisition of stack images as soon as the cell membrane was broken and the whole-cell configuration was established. Patch pipettes were filled with 143 mM KCl, 2 mM KOH, 1 mM EGTA, 10 mM HEPES, 0.3 mM $CaCl_2$, 0.5 mM NaGTP, 2 mM MgATP, and 10 μg/μl Rhodamin123. Cells were illuminated using the 488-nm line of an argon laser and the surrounding emissions (<350 μm) from 492 to 620 nm were detected.

The surgery and recording protocols are described in detail in the Supplemental Experimental Procedures.

Morphological Reconstruction and Immunohistochemistry

For reconstruction of the LFP electrode track and of the morphology of whole-cell recorded neurons, rats were deeply anesthetized with 10% ketamine (aniMedica)/2% xylazine (WDT) in NaCl (10 μg/g body weight, i.p.) and perfused transcardially with 4% paraformaldehyde. Tissue blocks containing the PL were sectioned in the coronal plane at 400 μm. The slices were stained for biocytin with Cyanine dye 2 (Cy2)-conjugated streptavidin and for GABA. For details, see the Supplemental Experimental Procedures.

Data Analysis

Data were imported and analyzed offline using MiniAnalysis software (Synaptosoft) and custom-written tools in MATLAB software version R2013b (MathWorks). For details, see the Supplemental Experimental Procedures.

Statistics

Statistical analyses were performed with SPSS Statistics 21 (IBM). Data were tested for normal distribution by the Kolmogorov-Smirnov test. Normally distributed data were tested for significant differences (*$p < 0.05$, **$p < 0.01$, and ***$p < 0.001$) using paired or unpaired t test. Not normally distributed data and datasets with $n < 10$ were tested with the non-parametric Mann-Whitney-Wilcoxon and Kruskal-Wallis tests. Mean ± SEM is stated to represent data in the text.

SUPPLEMENTAL INFORMATION

Supplemental Information includes Supplemental Experimental Procedures, seven figures, and one table and can be found with this article online at http://dx.doi.org/10.1016/j.celrep.2015.03.031.

AUTHOR CONTRIBUTIONS

I.L.H.-O. designed the experiments. S.H.B and K.D.S. carried out the experiments. K.S. and S.H.B. analyzed the data. K.D.S. and M.S. contributed to the establishment of experimental protocols. I.L.H.-O., S.H.B., and K.S. interpreted the data and wrote the paper. All authors discussed and commented on the manuscript.

ACKNOWLEDGMENTS

We thank Annette Marquardt and Achim Dahlmann for excellent technical assistance; Tobias Ackels for help with live imaging; as well as Drs. Werner Kilb, Jochen Roeper, and Thomas Oertner for helpful suggestions on the manuscript. I.L.H.-O. acknowledges support by the German Research Foundation (Emmy Noether Program, Ha4466/3-1; SFB 936, B5; SPP 1665, Ha4466/7-1).

Received: September 30, 2014
Revised: January 26, 2015
Accepted: March 11, 2015
Published: April 9, 2015

REFERENCES

Akam, T., and Kullmann, D.M. (2014). Oscillatory multiplexing of population codes for selective communication in the mammalian brain. Nat. Rev. Neurosci. *15*, 111–122.

Bartos, M., Vida, I., and Jonas, P. (2007). Synaptic mechanisms of synchronized gamma oscillations in inhibitory interneuron networks. Nat. Rev. Neurosci. *8*, 45–56.

Bitzenhofer, S.H., and Hanganu-Opatz, I.L. (2014). Oscillatory coupling within neonatal prefrontal-hippocampal networks is independent of selective removal of GABAergic neurons in the hippocampus. Neuropharmacology *77*, 57–67.

Blaesse, P., Airaksinen, M.S., Rivera, C., and Kaila, K. (2009). Cation-chloride cotransporters and neuronal function. Neuron *61*, 820–838.

Blatow, M., Rozov, A., Katona, I., Hormuzdi, S.G., Meyer, A.H., Whittington, M.A., Caputi, A., and Monyer, H. (2003). A novel network of multipolar bursting interneurons generates theta frequency oscillations in neocortex. Neuron *38*, 805–817.

Brockmann, M.D., Pöschel, B., Cichon, N., and Hanganu-Opatz, I.L. (2011). Coupled oscillations mediate directed interactions between prefrontal cortex and hippocampus of the neonatal rat. Neuron *71*, 332–347.

Buzsáki, G. (2002). Theta oscillations in the hippocampus. Neuron *33*, 325–340.

Buzsáki, G., and Wang, X.J. (2012). Mechanisms of gamma oscillations. Annu. Rev. Neurosci. *35*, 203–225.

Cardin, J.A., Carlén, M., Meletis, K., Knoblich, U., Zhang, F., Deisseroth, K., Tsai, L.H., and Moore, C.I. (2009). Driving fast-spiking cells induces gamma rhythm and controls sensory responses. Nature *459*, 663–667.

Chu, J., and Anderson, S.A. (2015). Development of cortical interneurons. Neuropsychopharmacology *40*, 16–23.

Cichon, N.B., Denker, M., Grün, S., and Hanganu-Opatz, I.L. (2014). Unsupervised classification of neocortical activity patterns in neonatal and pre-juvenile rodents. Front. Neural Circuits *8*, 50.

Clement, E.A., Richard, A., Thwaites, M., Ailon, J., Peters, S., and Dickson, C.T. (2008). Cyclic and sleep-like spontaneous alternations of brain state under urethane anaesthesia. PLoS One *3*, e2004.

Colonnese, M.T. (2014). Rapid developmental emergence of stable depolarization during wakefulness by inhibitory balancing of cortical network excitability. J. Neurosci. *34*, 5477–5485.

Colonnese, M.T., and Khazipov, R. (2010). "Slow activity transients" in infant rat visual cortex: a spreading synchronous oscillation patterned by retinal waves. J. Neurosci. *30*, 4325–4337.

Csicsvari, J., Hirase, H., Czurkó, A., Mamiya, A., and Buzsáki, G. (1999). Oscillatory coupling of hippocampal pyramidal cells and interneurons in the behaving Rat. J. Neurosci. *19*, 274–287.

Dupont, E., Hanganu, I.L., Kilb, W., Hirsch, S., and Luhmann, H.J. (2006). Rapid developmental switch in the mechanisms driving early cortical columnar networks. Nature *439*, 79–83.

Freund, T.F., and Antal, M. (1988). GABA-containing neurons in the septum control inhibitory interneurons in the hippocampus. Nature *336*, 170–173.

Hafting, T., Fyhn, M., Molden, S., Moser, M.B., and Moser, E.I. (2005). Microstructure of a spatial map in the entorhinal cortex. Nature *436*, 801–806.

Hanganu, I.L., Ben-Ari, Y., and Khazipov, R. (2006). Retinal waves trigger spindle bursts in the neonatal rat visual cortex. J. Neurosci. *26*, 6728–6736.

Hanganu-Opatz, I.L. (2010). Between molecules and experience: role of early patterns of coordinated activity for the development of cortical maps and sensory abilities. Brain Res. Brain Res. Rev. *64*, 160–176.

Hu, H., Gan, J., and Jonas, P. (2014). Interneurons. Fast-spiking, parvalbumin^{+} GABAergic interneurons: from cellular design to microcircuit function. Science *345*, 1255263.

Janiesch, P.C., Krüger, H.S., Pöschel, B., and Hanganu-Opatz, I.L. (2011). Cholinergic control in developing prefrontal-hippocampal networks. J. Neurosci. *31*, 17955–17970.

Karube, F., Kubota, Y., and Kawaguchi, Y. (2004). Axon branching and synaptic bouton phenotypes in GABAergic nonpyramidal cell subtypes. J. Neurosci. *24*, 2853–2865.

Khazipov, R., and Luhmann, H.J. (2006). Early patterns of electrical activity in the developing cerebral cortex of humans and rodents. Trends Neurosci. *29*, 414–418.

Kilb, W. (2012). Development of the GABAergic system from birth to adolescence. Neuroscientist *18*, 613–630.

Krüger, H.S., Brockmann, M.D., Salamon, J., Ittrich, H., and Hanganu-Opatz, I.L. (2012). Neonatal hippocampal lesion alters the functional maturation of the prefrontal cortex and the early cognitive development in pre-juvenile rats. Neurobiol. Learn. Mem. *97*, 470–481.

Krupa, M., Gielen, S., and Gutkin, B. (2014). Adaptation and shunting inhibition leads to pyramidal/interneuron gamma with sparse firing of pyramidal cells. J. Comput. Neurosci. *37*, 357–376.

Langston, R.F., Ainge, J.A., Couey, J.J., Canto, C.B., Bjerknes, T.L., Witter, M.P., Moser, E.I., and Moser, M.B. (2010). Development of the spatial representation system in the rat. Science *328*, 1576–1580.

Lee, A.T., Gee, S.M., Vogt, D., Patel, T., Rubenstein, J.L., and Sohal, V.S. (2014). Pyramidal neurons in prefrontal cortex receive subtype-specific forms of excitation and inhibition. Neuron *81*, 61–68.

Lisman, J.E., and Jensen, O. (2013). The θ-γ neural code. Neuron *77*, 1002–1016.

Minlebaev, M., Colonnese, M., Tsintsadze, T., Sirota, A., and Khazipov, R. (2011). Early γ oscillations synchronize developing thalamus and cortex. Science *334*, 226–229.

Nimmrich, V., Maier, N., Schmitz, D., and Draguhn, A. (2005). Induced sharp wave-ripple complexes in the absence of synaptic inhibition in mouse hippocampal slices. J. Physiol. *563*, 663–670.

Pernía-Andrade, A.J., and Jonas, P. (2014). Theta-gamma-modulated synaptic currents in hippocampal granule cells in vivo define a mechanism for network oscillations. Neuron *81*, 140–152.

Scheffer-Teixeira, R., Belchior, H., Leão, R.N., Ribeiro, S., and Tort, A.B. (2013). On high-frequency field oscillations (>100 Hz) and the spectral leakage of spiking activity. J. Neurosci. *33*, 1535–1539.

Schmitz, D., Schuchmann, S., Fisahn, A., Draguhn, A., Buhl, E.H., Petrasch-Parwez, E., Dermietzel, R., Heinemann, U., and Traub, R.D. (2001). Axo-axonal coupling. a novel mechanism for ultrafast neuronal communication. Neuron *31*, 831–840.

Sohal, V.S., Zhang, F., Yizhar, O., and Deisseroth, K. (2009). Parvalbumin neurons and gamma rhythms enhance cortical circuit performance. Nature *459*, 698–702.

Stark, E., Eichler, R., Roux, L., Fujisawa, S., Rotstein, H.G., and Buzsáki, G. (2013). Inhibition-induced theta resonance in cortical circuits. Neuron *80*, 1263–1276.

Vida, I., Bartos, M., and Jonas, P. (2006). Shunting inhibition improves robustness of gamma oscillations in hippocampal interneuron networks by homogenizing firing rates. Neuron *49*, 107–117.

Wang, X.J. (2010). Neurophysiological and computational principles of cortical rhythms in cognition. Physiol. Rev. *90*, 1195–1268.

Wang, Y., Markram, H., Goodman, P.H., Berger, T.K., Ma, J., and Goldman-Rakic, P.S. (2006). Heterogeneity in the pyramidal network of the medial prefrontal cortex. Nat. Neurosci. *9*, 534–542.

Womelsdorf, T., Valiante, T.A., Sahin, N.T., Miller, K.J., and Tiesinga, P. (2014). Dynamic circuit motifs underlying rhythmic gain control, gating and integration. Nat. Neurosci. *17*, 1031–1039.

Yang, J.W., Hanganu-Opatz, I.L., Sun, J.J., and Luhmann, H.J. (2009). Three patterns of oscillatory activity differentially synchronize developing neocortical networks in vivo. J. Neurosci. *29*, 9011–9025.

Yang, J.W., An, S., Sun, J.J., Reyes-Puerta, V., Kindler, J., Berger, T., Kilb, W., and Luhmann, H.J. (2013). Thalamic network oscillations synchronize ontogenetic columns in the newborn rat barrel cortex. Cereb. Cortex *23*, 1299–1316.

Yang, J.M., Zhang, J., Yu, Y.Q., Duan, S., and Li, X.M. (2014). Postnatal development of 2 microcircuits involving fast-spiking interneurons in the mouse prefrontal cortex. Cereb. Cortex *24*, 98–109.

Zhang, Z.W. (2004). Maturation of layer V pyramidal neurons in the rat prefrontal cortex: intrinsic properties and synaptic function. J. Neurophysiol. *91*, 1171–1182.